DIRAC NOTE 2001-03

Ionisation detector offline alignment for Ni 2000 data taking

A.López Agüera

Universidad e de Santiago de Compostela

Abstract

A method for offline alignment and calibration of the dE/dx detector is proposed. A sample of good pair events extracted from 240 millions of triggers is analysed. Main sources of misalignment are indicated and corrected. In particular the detector inhomogeneities and the effect of the particle impact position along the detector element. A special treatment is applied to uniformize pairs correlated and not correlated in time. The contamination of single particles into the double ionisation sample is calculated after the corrections improvement.

An optimised cut is proposed after some considerations about differences between the relative momentum distributions for single and double ionisation events. The alignment method is generalised to the Platinum 1999 data.

Contains

1.- Problem definition
2.- dE/dx signal characteristic.
  2.1 Number of photoelectrons.
  2.2 Detector linearity.
  2.3 Single-Double ionisation separation capability.
3.- Detector homogeneity alignment
4.- Impact Position dependence alignment
  4.1 Dependence along the counter (Y co-ordinate)
  4.2 Signal detector maps(X co-ordinate)
5.- Time dependence.
6.- Momentum and charge dependences.
7.- LayerA-LayerB predictions comparison
8.- Improvements after corrections
9.- Cut criteria(considerations about Q).
10.- Comparison with Platinum 99 data.
11.- Conclusions.

10 May 2001

1 Problem definition

The dE/dx detector has been designed [1,2,3,4] to identify pairs of particles crossing the sensitive area close in space and time. The ionisation produced will be proportional to the number of particles hitting each detector element.A simple cut will allow us to distinguish single from double ionisation signal. An accurate uniformity of the signal collected after the PMT is required to avoid systematic effect into the final results. The process to correct any inhomogeneity is called *detector alignment*. The figure 1 shows the main sources of misalignment which can be resumed as:

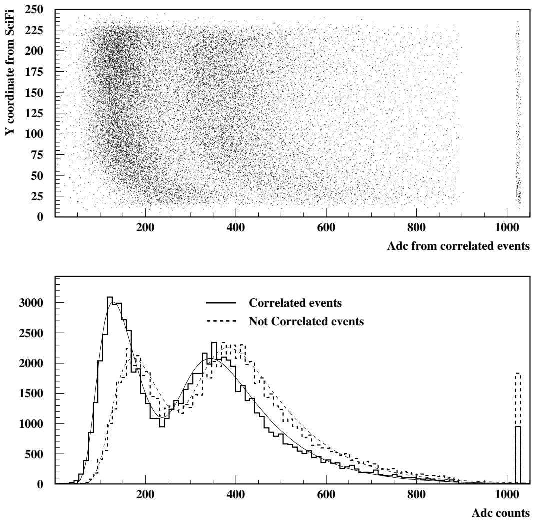

Fig. 1. Top ADC distribution dependence with the impact position of the particle along the detector. On the bottom ADC distribution for correlated and not correlated events.

a.- **Detector homogeneity** due to the structural differences between detector elements.

b.- **Impact position dependence in both X and Y co-ordinates.** , where the X dependence appears correlated with the interspace between detector elements. The Y co-ordinate is due to a loss of focussing when the particle hit the detector close to the light-guide.

c.- **Time dependence** associated to a not optimised readout gate definition.

Finally, the study is performed over a sample of **Good pair events** correlated and not correlated extracted from 240 millions of trigger acquired during the 2000 Spring run. The target is Nickel. An additional condition is required: the difference in the number of fibers fired is different from zero.

2 dE/dx signal characteristic

Figure 2 shows the typical shape of dE/dx output signal. Main parameter defining the detector performance are indicated. In particular:

a.- The number of photoelectrons.
b.- The linearity in the response.
c.- The single-double ionisation separation capability.

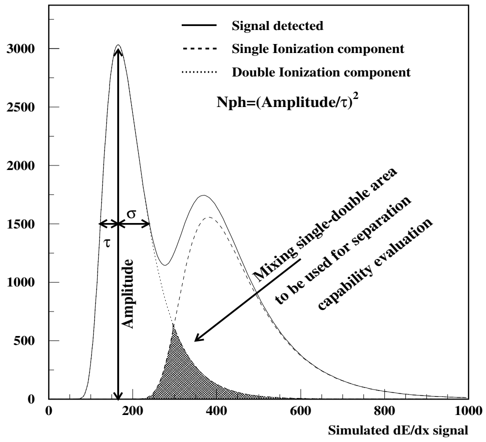

Fig. 2. Output signal simulated for dE/dx detector.

It is supposed that the signal is well described by a double Landau distribution, as shown in the figure.

2.1 Number of photoelectrons

The number of photoelectrons(Nph) is defined as :

$$\sqrt{N}ph = \frac{A}{\tau} \tag{1}$$

where A is the Landau mean value and σ the corresponding width, or more strictly the width obtained by the process to *gaussianize* the landau distribution. The A value need to be corrected by the ADC pedestal and online suppression.

2.2 Detector linearity

In principle, the detector is expected to give a linear response with the energy deposited. If it is true we can write :

$$\frac{D+C}{S+C} = \sqrt{2}\frac{\tau d}{\tau s} \tag{2}$$

where S and D represent the single and double mean values of the Landau peak, τs and τd the corresponding widths for the gaussian fit. C takes into account the pedestals and online suppression.

The linearity hypothesis allow us to obtain C for our sample:

$$C = 48 \pm 6 ADCcounts. \tag{3}$$

2.3 The single-double ionisation separation capability

The detector capability to separate single and double ionisation signal is computed by measuring the intersection area between both Landau distributions corresponding to single and double ionisation signal.

The first step of analysis will be to try to evaluate how a Landau fit is appropriate to describe the detector signal. Let us separate single and double ionisation sample using the ScFi position information. We define:

$$\Delta(X) = X_{ScFi}(1) - X_{ScFi}(2) \tag{4}$$

where $X_{ScFi}(i)$ correspond to the X co-ordinate of particle i in the pair.

Figure 3 shows the ADC dE/dx distribution for several $\Delta(X)$ intervals. Note the effect of the cut on the percentage of single and double ionisation populations.

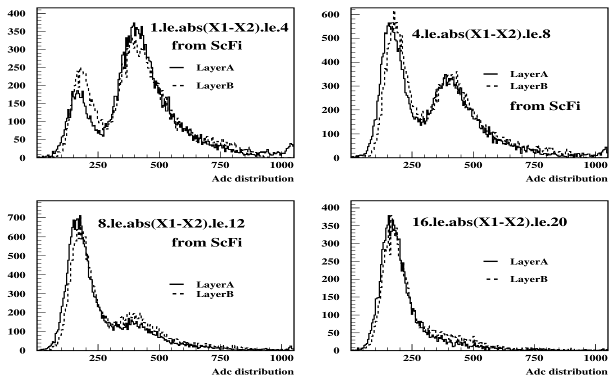

Fig. 3. ADC distribution for different $\Delta(X)$ interval.

The following definitions seem acceptable:

1.- **Single ionisation sample:** We select $\Delta(X)$ larger than the dE/dx element size. Practically, $\Delta(X)$ larger than 18 fibers which correspond to 0.88cm.

2.- **Double ionisation**: We select $\Delta(X)$ as small as possible, in other words both particles as close as possible. In fact, $\Delta(X)$ is defined to be equal to 2 fibers, which correspond to 0.09cm particles separation.

Fig. 4. ADC distribution when Single ionisation events are selected.

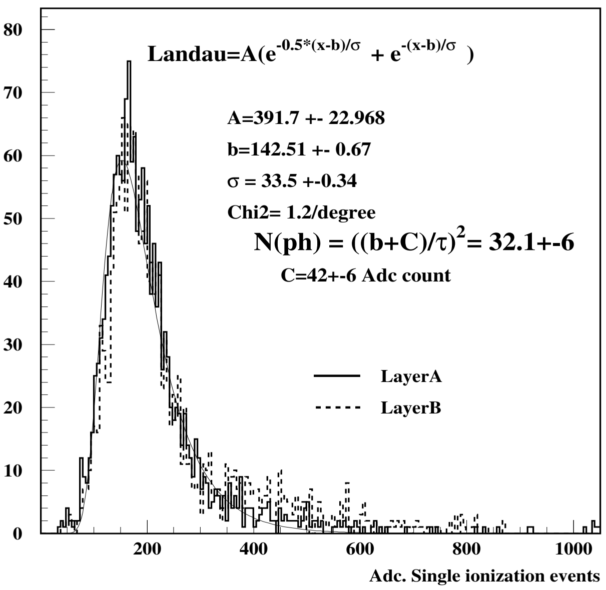

Figure 4 shows the ADC distribution for the single ionisation mfitted by a single Landau curve defined as:

$$Landau = A(e^{0.5*(x-b)/\sigma} + e^{-(x-b)/\sigma}) \tag{5}$$

where A is the normalisation factor, b the most probable value and σ the Landau distribution width. The number of photoelectrons obtained is 32.1 ± 6.

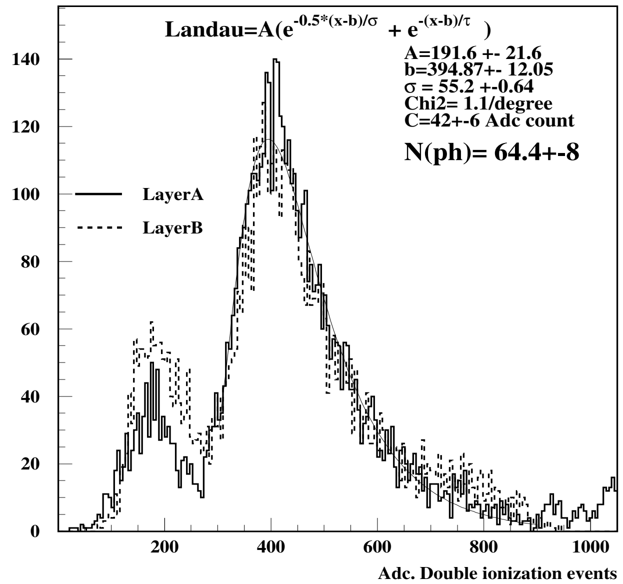

Fig. 5. ADC distribution when Double ionisation events are selected.

As before, figure 5 shows the ADC distribution for double ionisation sample. The number of photoelectrons collected is 64.4 ± 8 in this case. We can conclude that a Landau distribution describes in a rather accurate way the dE/dx signals and will be considered a good approximation to estimate the detector separation capability.

3 Detector homogeneity alignment

Each detector element suffer from the peculiarities of its components. The scintillator plastic transmission light, the quality of the gluing process, the transmission time of PMT are good examples. The readout electronic can not be neglected. Every of the parameters mentioned induce inhomogeneities in the global detector response and need to be corrected.

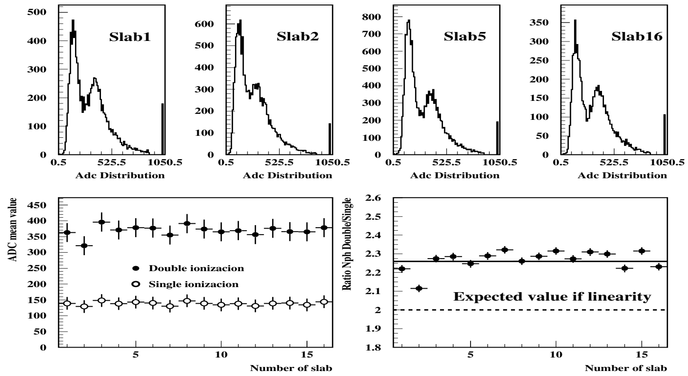

Fig. 6. LAYER A:On top, ADC distribution for different slabs. At the bottom-left, mean value from the Landau distribution for single and double ionisation. Bottom-right the ratio between the numbers of photoelectrons computed for single and double ionisation.

Figure 6 and 7 illustrate the ADC distribution behaviour for several elements in both A and B dE/dx layers. No strong differences are observed. Only the non standard behaviour of element 2 in layer A is perceptible. As a further remark, even if the linearity is conserved, the distribution width looks 30 % wider than the one observed for the rest of detector elements.

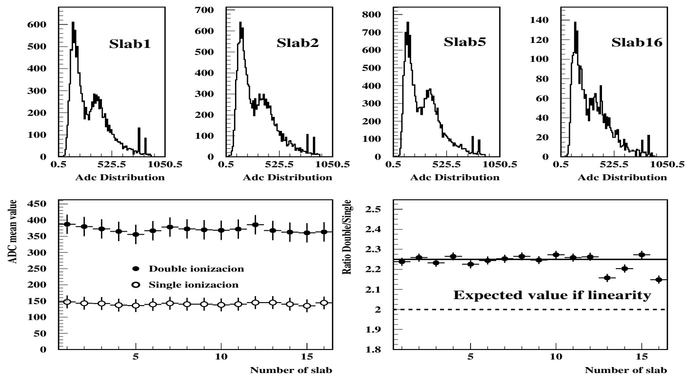

Fig. 7. LAYER B: On top, ADC distribution for different slabs. At the bottom-left, mean value from the Landau distribution for single and double ionisation. Bottom-right the ratio between the numbers of photoelectrons computed for single and double ionisation.

But the most important result we can get from the previous figures is how similar are the widths of the distributions for both single and double ionisation element to element:

$$\sigma_S = 40 \pm 4; \sigma_D = 56 \pm 5 \tag{6}$$

where σ_s and σ_d are the corresponding single and double Landau width. The table I contains the 32 proposed corrections:

		1	2	3	4	5	6	7	8	9	10	11	12	13	14	15	16
	A	0	10	-9	1	-4	-1	9	-8	0	5	1	8	0	-1	5	-5
	B	-7	-3	-2	3	4	1	-3	0	0	2	0	-5	-5	0	5	-4

Table 1
Correction for each element of dE/dx detector in ADC counts

3.1 Correction application

To propose a correction method it is needed to notice two facts: the stable observed linearity and the uniform distributions width. As said before, the elements parameters are similar within a 10 % of tolerance.

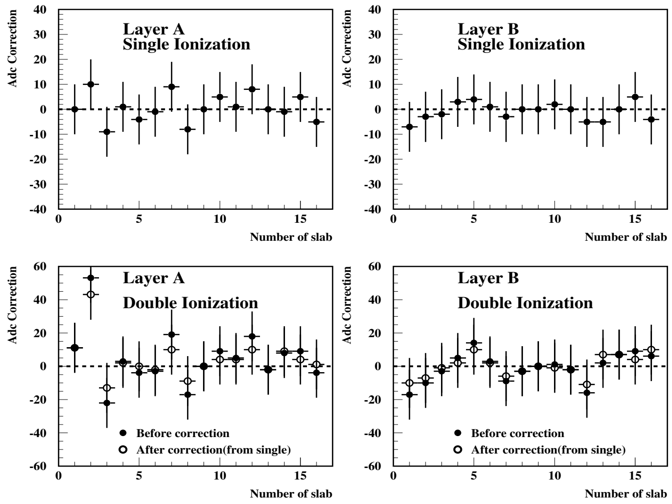

Fig. 8. On top, the correction for single ionisation computed for both layers. At the bottom the ADC mean value for double before and after corrections.

In these conditions, the simplest method we can imagine is to apply a translation in the way follows:

$$\mathbf{ADC_i = ADC_i(measured) - Correction(Slab(i))}, \ i = 1, ..., 16 \tag{7}$$

where the correction, $Correction(Slab(i))$, has been obtained using the element 9 from each layer as reference.

4 Impact position dependence

4.1 Dependence along the counter (Y co-ordinate)

When a particle crosses the scintillator element close to the light-guide we observe a strong increase of the detected signal peak without modification in the Landau width. An effect due to light attenuation can give a plausible explanation for the lost of photoelectrons.

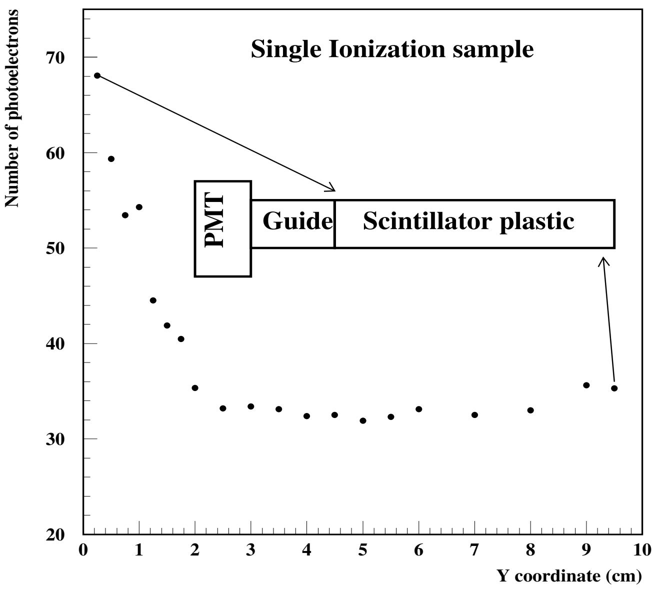

Fig. 9. Symbolical description of the observed misalignment

Just to clarify the problem and in a symbolic way, figure 9 illustrate the observed effect.

The impact point of the particle along the Y co-ordinate is defined using the SciFI detector information. Fiber detector granularity fulfils the precision needs. Both detectors are close enough to be used as a good position approximation. By definition, the zero of the distribution is fixed close to the light-guide.

4.1.1 Method to correct:

The method proposed is the following:

1.- **ADC distribution is fitted using a double Landau for different Y intervals**. Each interval correspond to 1cm of scintillator plastic.

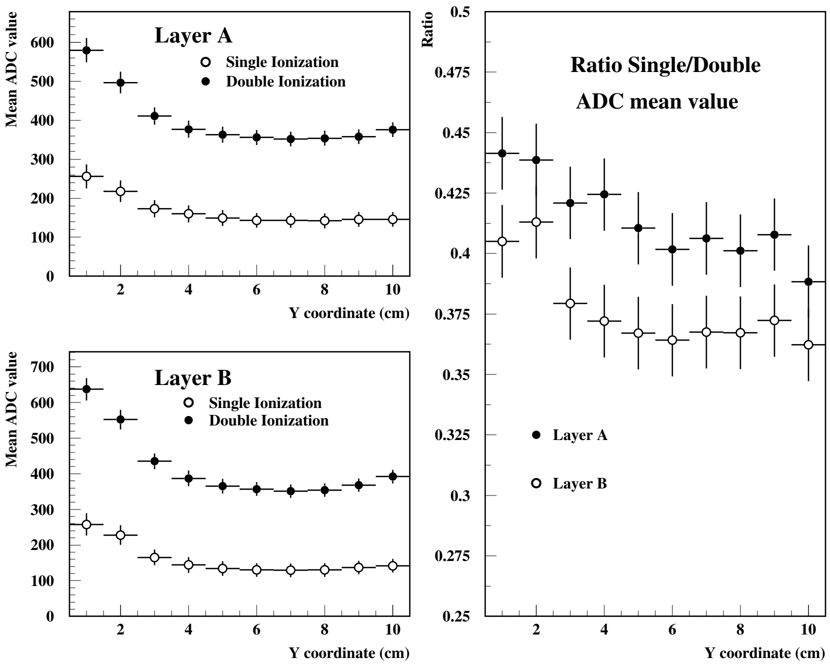

Fig. 10. Mean value from single and double ionisation dependence with the impact position of the particle. On the left, top for layer A and bottom for layer B. On the right, ratio between single and double ionisation mean values for both A and B layers

Figure 10 shows how the dependence look for both A and B layers respectively. In the right part of the same figure the ratio between single and double ionisation ADC value is shown. The small inclination detected allow us to applly the same criteria to correct every signal.

2.- **The Mean ADC values dependence from the Y co-ordinate are fitted using a polynomial**, separately for single and double ionisation defined as:

$$P^3(Y) = a_0 + a_1 * Y + a_2 * Y^2 + a_3 * Y^3 \qquad (8)$$

where a_0, a_1, a_2 and a_3 are the parameters obtained from the fit procedure. Only a_0 is fixed depending on the kind of signal concerned.

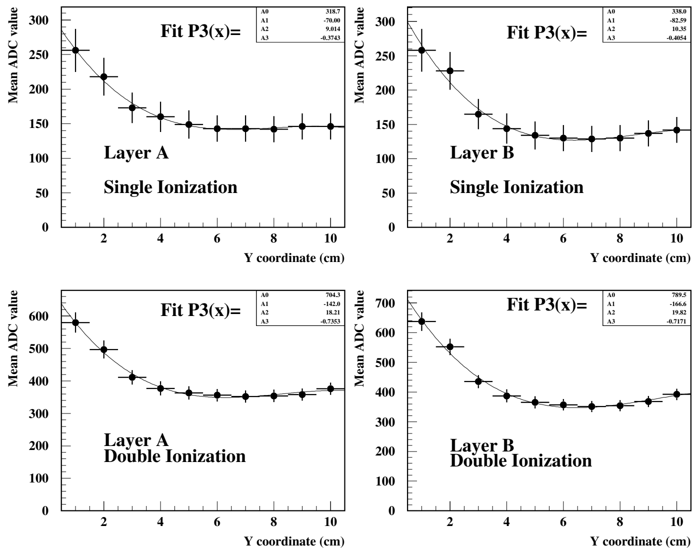

Fig. 11. Polynomial fits for each of the ADC mean value distributions.

Table II contain the a_0 values for single and double ionisation signals. In practice, a_0 will represent the value of the separation cut defined.

	Single	*Double*
Layer A	318.±5	704±12
Layer B	338.±6	779±12

Table 2
a_0 values obtained from the polynomial fit.

The a_1, a_2 and a_3 parameter values are shown in table III. The quoted errors are obtained from the fit procedure.

In all cases, the results for both A and B layers are in good agreement within errors.

	a_1	a_2	a_3
$Layer A$	-70.±2.5	9.17±1.06	-0.40±0.05
$Layer B$	-68.±2.4	10.4±1.3	-0.37±0.05

Table 3
Parameters from the $P^3(y)$ fit for single ionisation signal.

3.- **The fit parameters are used to redefine the** *cut* Cut_{S-D} determined in order to separate single and double ionisation in the standard analysis in the following way:

$$Cut_{S-D} = Cut_{S-D}(defined) - P^3(Y) \tag{9}$$

where Y represent the particle impact position and $Cut_{S-D}(defined)$ will be determined in order to optimise the compromise between high statistic and a small fraction of single contamination on the double ionisation sample.

4.1.2 Results

Figures 12 and 13 show the ADC distributions for several impact position intervals for both layers separately. The last picture in each, corresponding to the end of the scintillator plastic, evidence for a strong decrease of double ionisation population. A simple shows an cutting edge effect can give a consistent explanation.

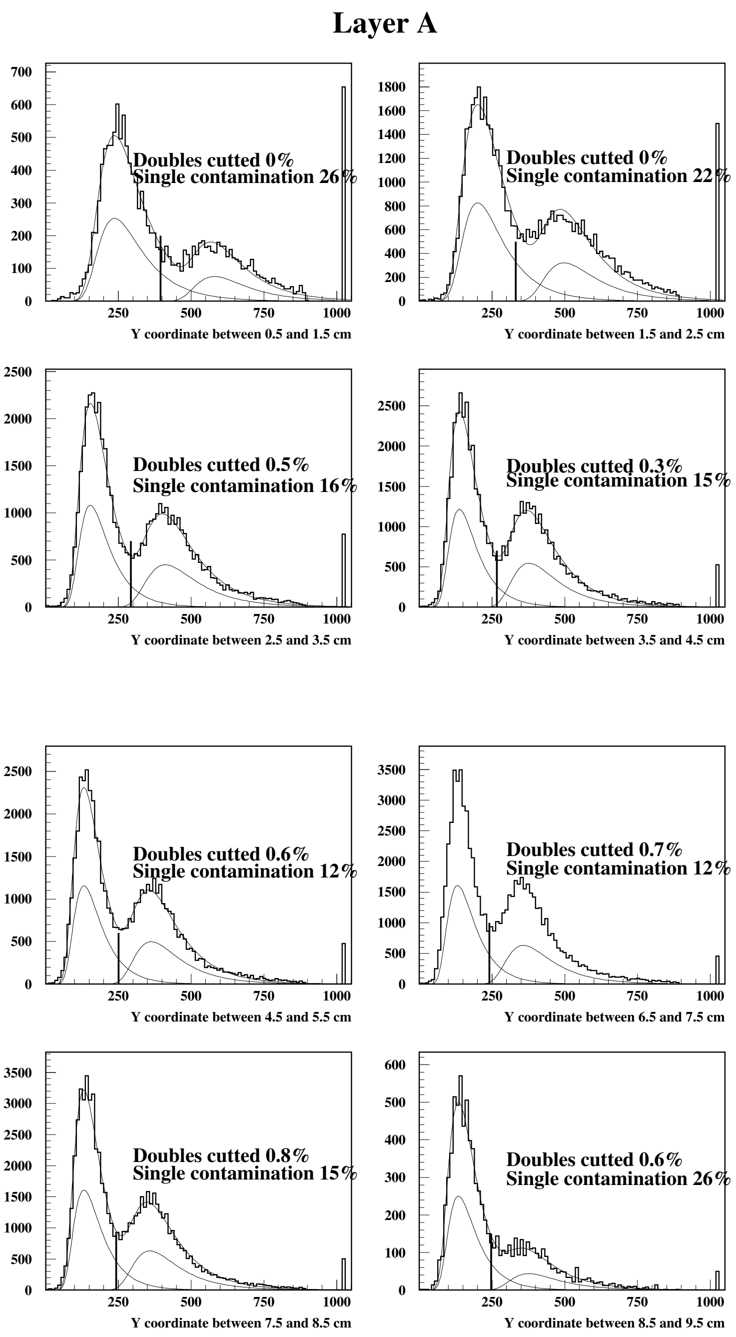

Fig. 12. LAYER A:ADC distribution for different impact position intervals. The 2 different Landau distributions correspond to single and double ionisation. The line is the cut between single and double.

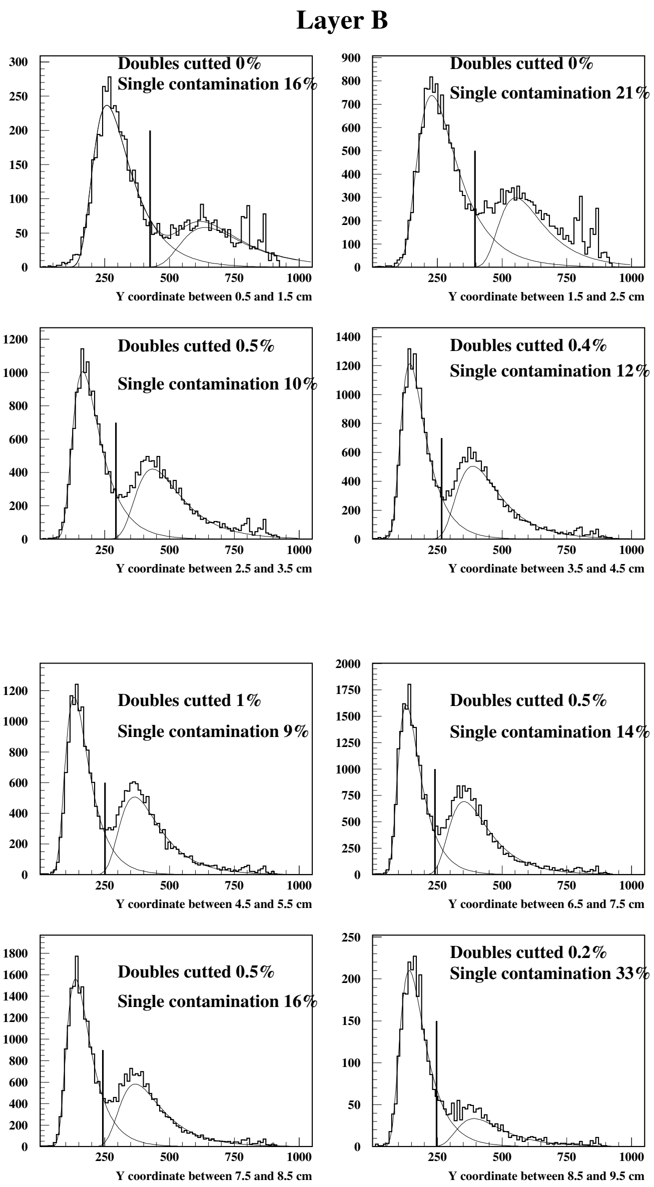

Fig. 13. LAYER B:ADC distribution for different impact position intervals. The 2 different Landau distribution correspond to single and double ionisation. The line is the cut between single and double.

In figure 14 the percentage of single contamination as well as the fraction of double ionisation loss are shown. A rather conservative separation cut value has been used (Cut_{S-D}=250 ADC count). The criteria was to avoid any loss of statistics. Finally figure 15 shows the similar behaviour found when correlated and no-correlated events are singly analysed.

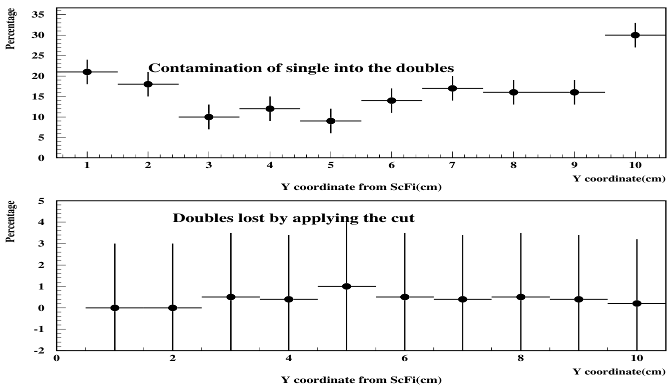

Fig. 14. On top the contamination of single ionisation in the double ionisation sample. On the bottom the percentage of double signal rejected by the cut.

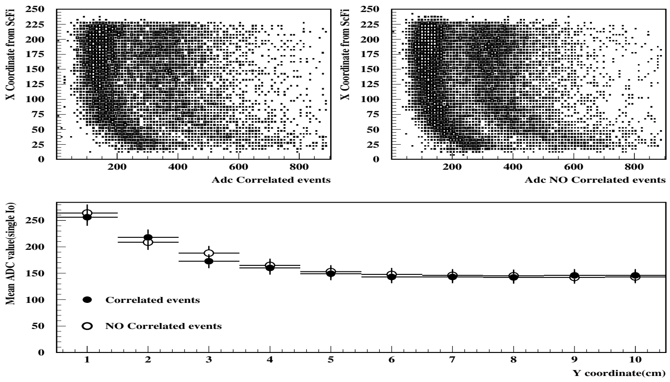

Fig. 15. On top scatter-plot of ADC distribution versus the Y co-ordinate computed using the SciFi position for both correlated and not correlated events. On the bottom the same distribution but showing the ADC mean values.

4.1.3 Validity of the correction along time during the run

Finally, even if not less important, some study about the validity of the proposed method along time is need. The equivalence between validity of the method and the signal detector stability is evident. But this last characteristic is much easier to control.

So, a variable is defined to pursue this purpose:

$$\eta = \frac{ADC_{meanvalue}(y \leq 1cm)(N_{run})}{ADC_{meanvalue}(y \leq 1cm)(N_{run} = 2152)} \tag{10}$$

where the run number 2152 has been taken as reference. Figure 16 shows the rather good stability in the sample which corresponds to about one month of normal data taking. Probably this variable can be consider as a good candidate

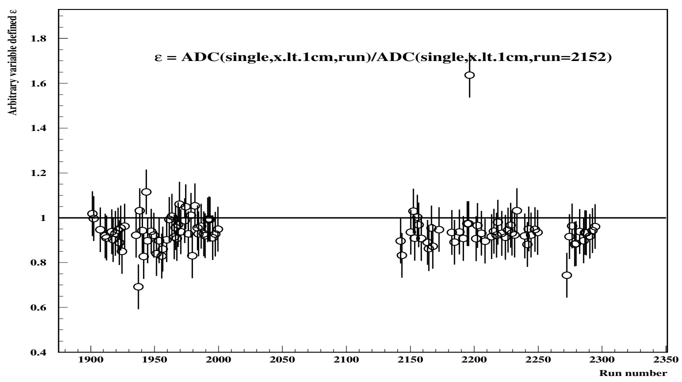

Fig. 16. *Arbitrary variable defined to control the detector stability along the time. Time unit is the run number*

to control the detector stability during the data-taking period. Obviously an element by element study will be mandatory.

4.2 Signal detector map(X co-ordinate)

The well defined space correlation between the ScFi and the dE/dx detectors (see figure 17 left side) allows us to perform a detailed map of the detector. The high granularity of ScFi permits a rather fine estimation of the interspaces existing between dE/dx adjacent elements. The main origin of these gaps comes from the scintillator wraping. The evidence is shown in figure 17 where the ADC counts from dE/dx are plotted with respect to the number of the fiber fired. In figure 18 the signal population in dE/dx is shown with respect to the number of the fiber fired. The histogram bin used corresponds to 2 fibers.

The shift introduced between both A and B layers in order to avoid the interspace effect is made evident. As conclusion **A criteria asking for double ionisation signal in at least one of both layer will ensure a low detection inefficiency**.

On the bottom of the same figure, the typical signal distributions for particles hitting the dE/dx detector in the center of a scintillator slab and or the border are shown. Notice the diminution of the capability to identify double

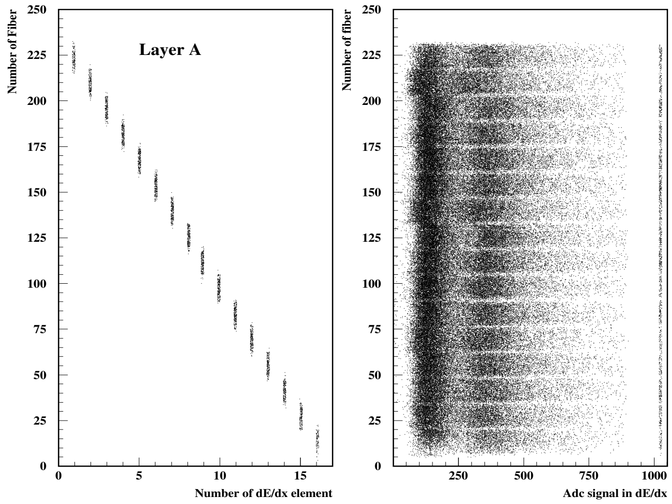

Fig. 17. *On the left dE/dx, ScFi detectors spatial correlations. On the right the space between adjacent detector elements are shown*

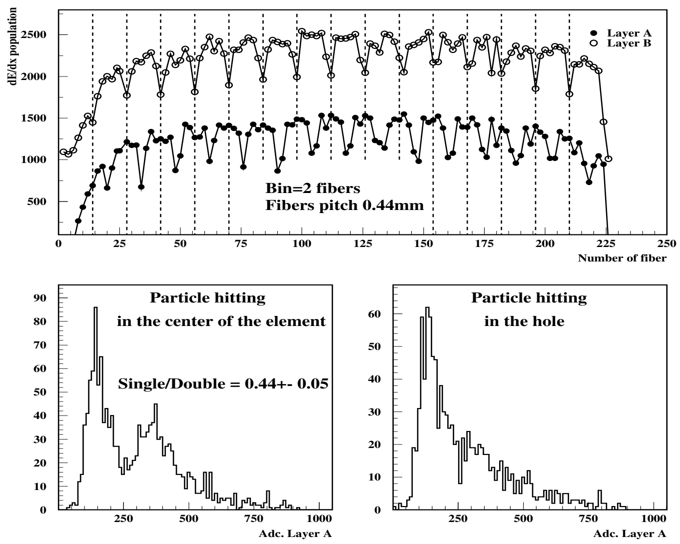

Fig. 18. *On the top, dE/dx population versus the number of fiber fired. On the bottom two typical signal distribution in the case of a particle firing in the center of a element or in the border respectively.*

ionisation signal when one of the particles hit the detector near by a gap. The expected fraction of failures can be theoretically estimated as about 10 %. A more precise experimental measure will be given afterward.

5 Time dependence

During 2000 data-taking an asymmetry appears between correlated and not correlated events. Moreover, a dependence of the ADC distribution with the time difference between the 2 particles from the pair is observed, as shown in figure 19.

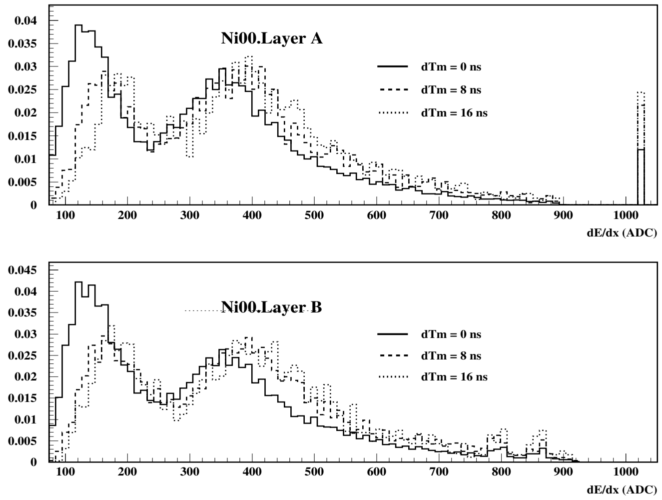

Fig. 19. *ADC distribution for pairs of particles arriving to the detector with different time intervals between the particles*

5.1 Possible explanation

The explanation is based on the read-out gate reduction applied at the beginning of 2000 data-taking. In effect, the actual gate is set to 56 ns instead of 70 ns last year[6].

The readout gate starts always with **T1*VH1** signal. The fixed dE/dx signal delay Δ has been optimised to put the dE/dx signal at the end of the defined ADC gate. For 2000 data-taking apparently only the gate width was changed while Δ remained stable.

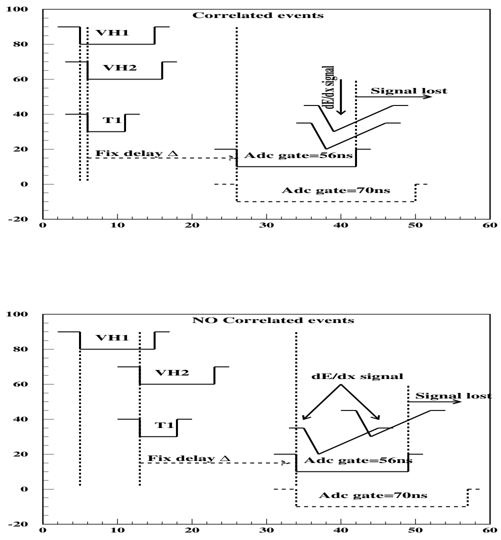

Fig. 20. *Symbolical description of the observed misalignment*

Figure 20 describes up symbolically the effect for correlated and not correlated events. When both particles in the pair that arrive to the detector correlated are a moderate fraction of signal is lost. When the particles coming in are not correlated in time, the ones arriving earlier can be fully contained in the ADC gate.

To verify the consistency of the previous hypothesis a dedicated run was taken with 70 ns ADC gate width. **(see run 2864)**.

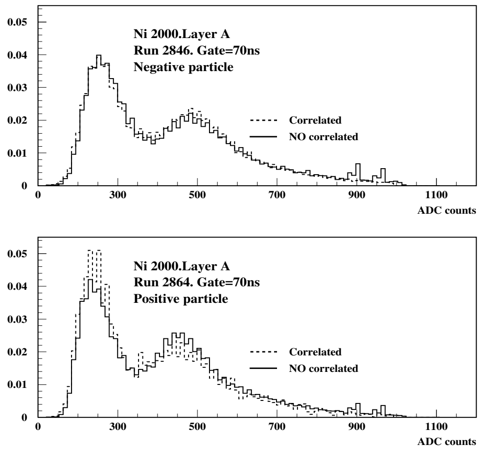

Fig. 21. *ADC distribution for correlated and not correlated events when the readout gate is 70 ns*

No discrepancies between correlated and not correlated pairs are observed as shown in figure 21, if so the loss of signal is correlated with a not optimised definition of dE/dx signal delay. **The question to clarify is if would be more efficient either to enlarge the ADC gate or to optimise the dE/dx signal delays.**

5.2 Correction method:

The correction method proposed is similar to the one established for the position dependence: signals are fitted using a double Landau distribution and the mean values are fitted using a polynomial curve. $P^1(abs(dTm))$ is obtained(see figures 22 and 23). Figure 24 shows on the top the results of the fit. A rather

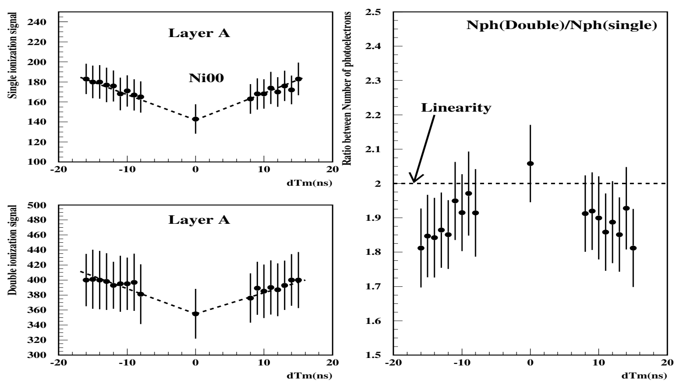

Fig. 22. *LAYER A: On the left Mean ADC value dependence with the time difference between particles for single (top) and double(bottom) ionisation. On the right the ratio between the numbers of photoelectrons collected for single and double ionisation.*

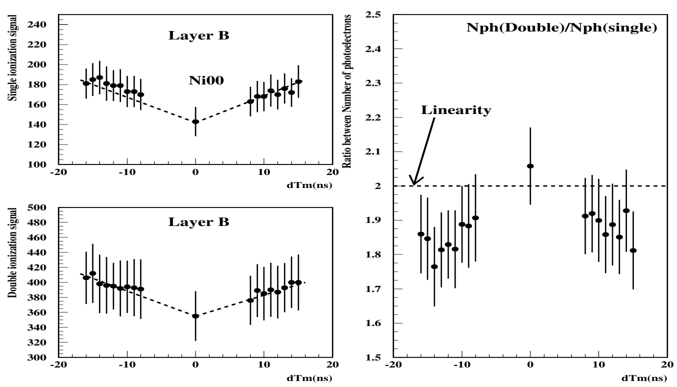

Fig. 23. *As figure 21 for LAYER B.*

good agreement is observed for either positive and negative difference of time intervals.

5.3 Results

Again, as in the previous case, the cut defined to separate double ionisation signal from single Cut_{S-D}, will be rewritten as:

$$CutS - D = CutS - D(defined) - P^3(Y) - P^1(abs(dTm)) \qquad (11)$$

where the Y *co-ordinate* is the impact parameter position from ScFi information in cm and dTm represents the time separation between the two particles from the pair in ns.

On the bottom part of figure 24 the single contamination is shown. The uniformity can be consider satisfactory.

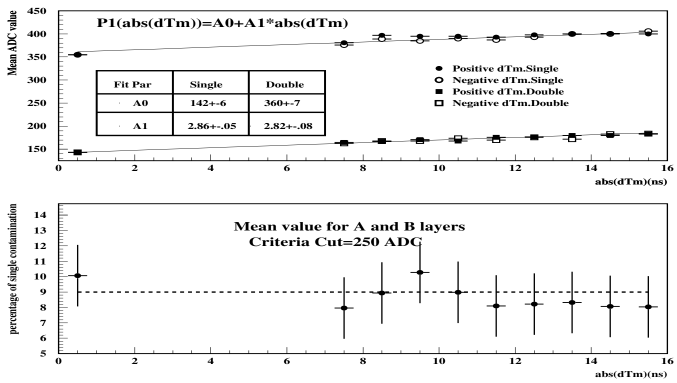

Fig. 24. *On the top, fit parameters obtained. On the bottom, contamination of single in doubles depending on the time difference between the 2 particles arriving to the detector*

6 Momentum and charge dependence

By definition, the detector response dependence with either the charge or the momentum of the particle in the experiment range need to be unsubstantial. Figures 25 and 26 show the good agreement for both correlated and not correlated events when several momentum intervals are selected between positive and negative particles.

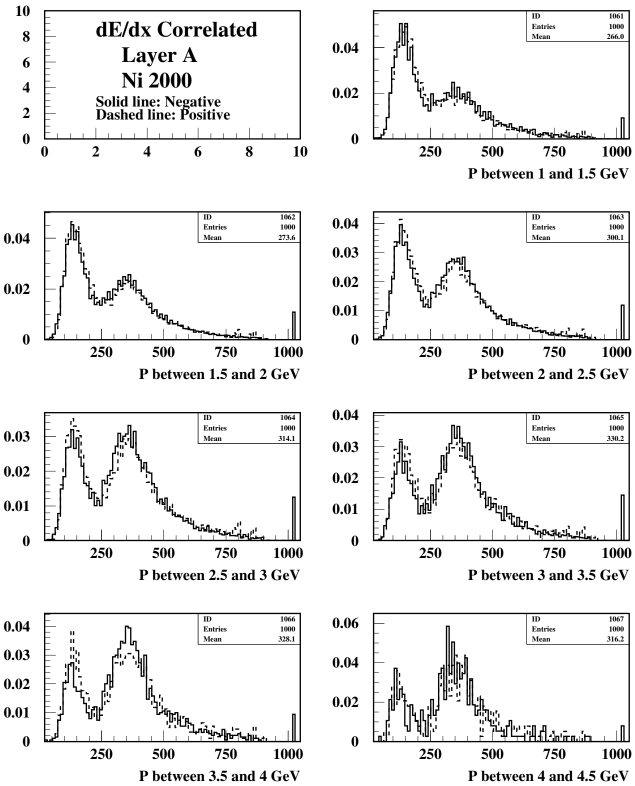

Fig. 25. *ADC distribution for positive and negative particles from correlated events.*

7 Layer A- Layer B predictions comparison

For the standard analysis a compromise between both A and B layer independent predictions is used as selection criteria. We try to estimate the percentage of identical answers as well as evaluate the causes of disagreement.

Again we need to use the ScFi position determination to define :

$$D = \sqrt{(X_1^{ScFi} - X_2^{ScFi})^2 + (Y_1^{ScFi} - Y_2^{ScFi})^2} \qquad (12)$$

where the co-ordinates are defined from the ScFi detector position determination. The subindex 1 and 2 correspond to both particles in the pair. The distance **D** varies between 0 and 1 cm in our sample. Cases where either $\Delta(X)$ or $\Delta(Y)$ are zero are rejected.

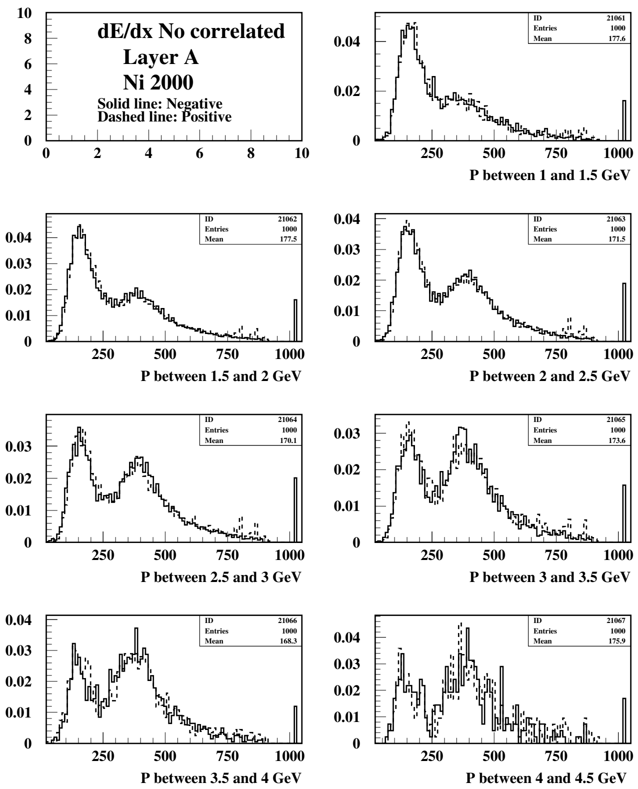

Fig. 26. *ADC distribution for positive and negative particles from not correlated events.*

We define two categories:

1. *Distance* **D** *greater than 0.8 cm.* Both particles are separated more than the dE/dx granularity. The events must be seen as single ionisation.
2. *Distance* **D** *smaller than 0.1 cm.* Compatible with double ionisation events.

7.1 Single ionisation hypothesis

Figure 27 try to summarise the information we get:

a. The difference between the signal detected in both layers (ADC(LayerA)-ADC(LayerB)) shows how in 23 % of the cases both layers give an opposite response.

b.- ADC distribution on layer A is plotted when layer B signal is smaller than 200 ADC counts, that is single ionisation compatible. The excess observed at high signal it not compatible with a Landau tail.

b. Both Q and Qt distributions are compatible with single ionisation events, as expected.

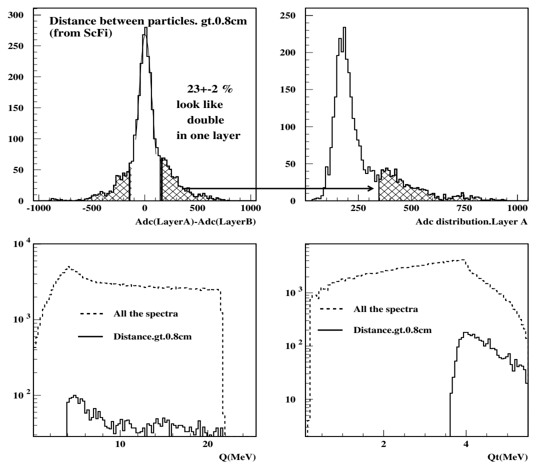

Fig. 27. *Using the single ionization hypotesis from Fiber detector, the dE/dx prediction is checked.*

The possible causes:

a.- Some pileup effect from a previous event.
b.- A second particle not detected by fibers.

7.2 Double ionisation hypothesis

We repeat the previous exercise for double ionisation hypothesis(see figure28):

a. Layer A and layer B give opposite responses in 34.4 % of cases.
b.- Again layer A is plotted when layer B signal is higher than 250 ADC counts, compatible with double ionisation criteria.
c. Qt distribution is compatible with double ionisation events.

The two possible explanations we can imagine are:

a.- Gaps or interspaces between detector elements .
b.- Two adjacent element are fired .

Let us try to evaluate the contribution of each type. The easiest way we can imagine to avoid the case when two adjacent elements are fired is to study the global ADC contribution per layer. In other words, plot the sum of the signals deposited for both particles in the same layer. Figure 29 shows the corresponding distribution both for single and double ionisation hypothesis.

The most important remark is how in both hypotheses a single ionisation compatible signal appears in 14% of cases. This number quotes rather accurately the percentage of particles lost in the detector gaps.

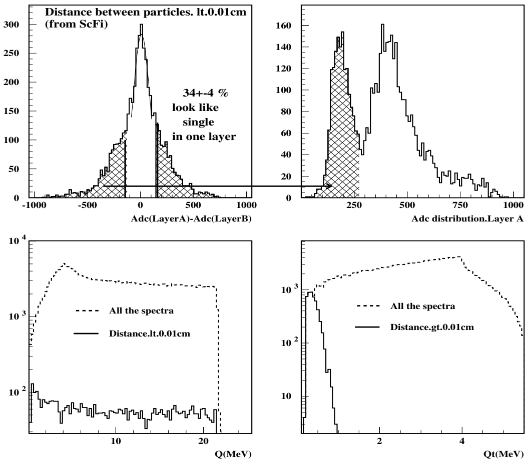

Fig. 28. *Using the double ionization hypotesis from Fiber detector, the dE/dx prediction is checked.*

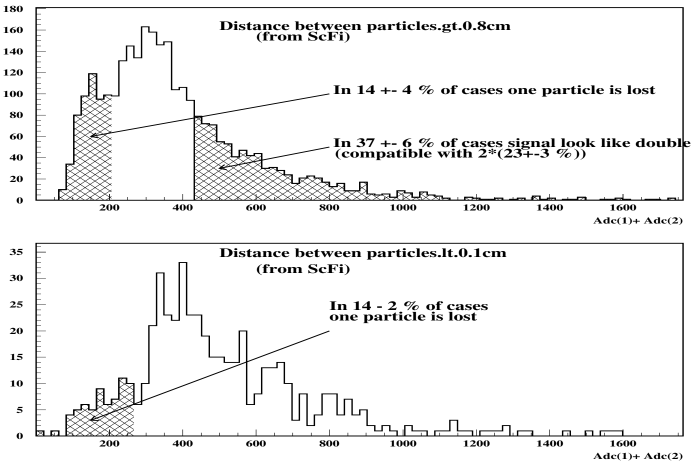

Fig. 29. *Layer A- Layer B predictions for single ionisation events.*

We can conclude that 7% of the particles firing the detector are lost per layer into the detector interspaces. This number is smaller than the geometrical estimation due to the fact than the incident angle is not 90 degrees for the particles crossing the sensitive area. Finally, in 10% of the cases, always per layer, both pair components fire two adjacent dE/dx elements.

8 Improvement after corrections

The goal pursue with the detector alignment process was double:

1.- Improve the global signal performance in order to decrease the single contamination in the double ionisation sample.
2.- Uniformize the signals coming from correlated and not correlated events.

The results obtained with respect to the first point are shown in figure 30. In effect, when all the corrections are applied correlated and not correlated events can be consider identical. The second goal is much more delicate. In principle

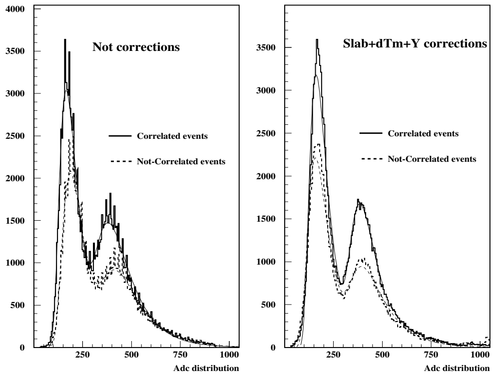

Fig. 30. *ADC distribution comparison for correlated and not correlated events.On the left before any correction. On the right when all the corrections have beenapplied.*

the simplest way to evaluate how much our detector is able to separate single from double ionisation improves is to measure the distributions widths. Figure 31 shows the corresponding sigma values when the various corrections are applied.

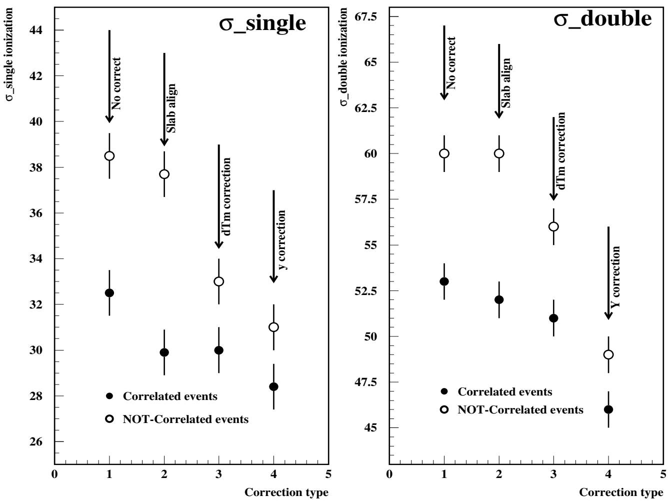

Fig. 31. *Width(obtained from the fit to the Landau distribution) variation when the different types of corrections are applied. Again Y correction means Slab alignment + time correction + position correction.*

The main remarks can be resumed in the following way:

a.- For not correlated events the time dependence correction is dominant. The signal distribution width is improved by $15 \pm 3\%$.

b.- Position dependence correction decreases the signal distribution width by 6 ± 2 %, independently of the kind of events we are looking at.

Let study separately the effect of the corrections into the correlated and not correlated on time event samples.

8.1 Correlated events

Figures 32 shows the ADC distribution signal for correlated events when different corrections are applied.

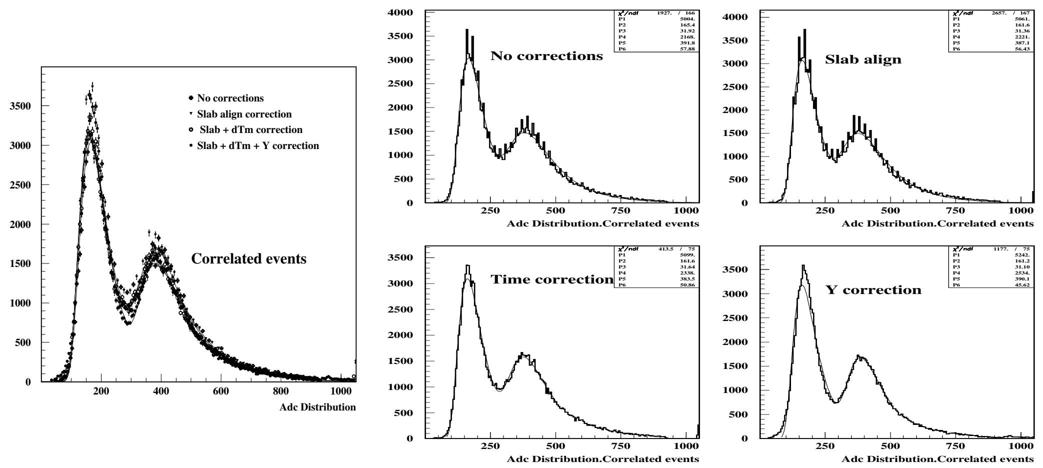

Fig. 32. *ADC distribution for correlated events when different corrections are applied.* **Remark:** *The corrections are added. This mean that Time corrections are applied after the corresponding slab alignment, and so on.*

As expected the signal after corrections is narrow for both single and double ionisation and the valley between is made evident. One of the parameter to optimise is the contamination area where the detector is not able to separate single from double ionisation.

Figure 33 shows the effect of the corrections applied over the common area for single and double ionisation. As it is shown in the included table, the single contamination is reduced by a factor of 2.

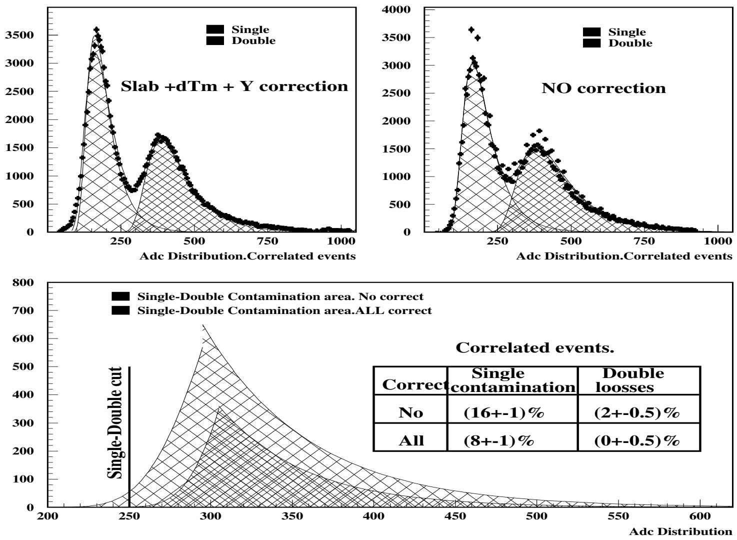

Fig. 33. *The common area between single and double ionization signal are shown before and after corrections.*

8.2 No Correlated events

Figure 34 shows the effect of the corrections applied ower the no correlated on time sample. As expected, the time correction become essential because the time interval between both particles into the pair varies from 6 to 16 ns.

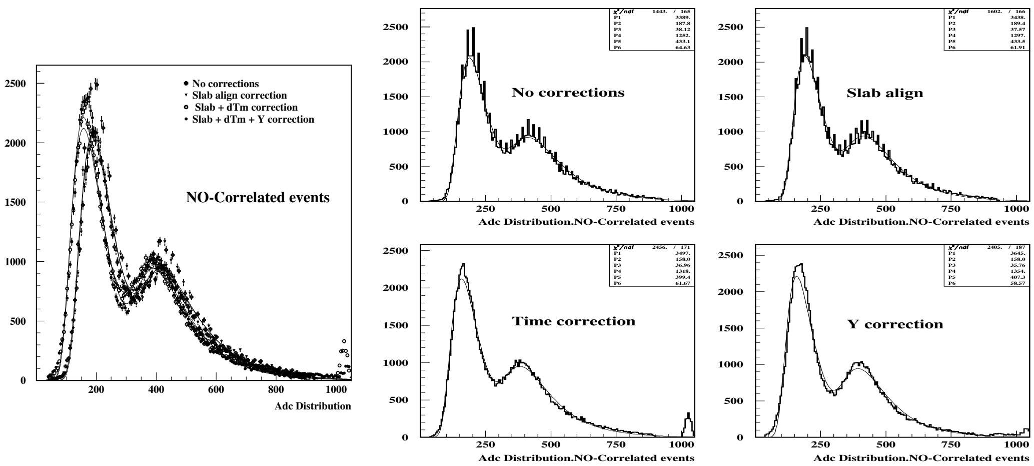

Fig. 34. *ADC distribution for correlated events when different corrections are applied*

Figure 35 shows the effect of the corrections applied over the common area for single and double ionisation. As it is shown in the included table, the single contamination is reduced by a factor of 2, as in the previous case.

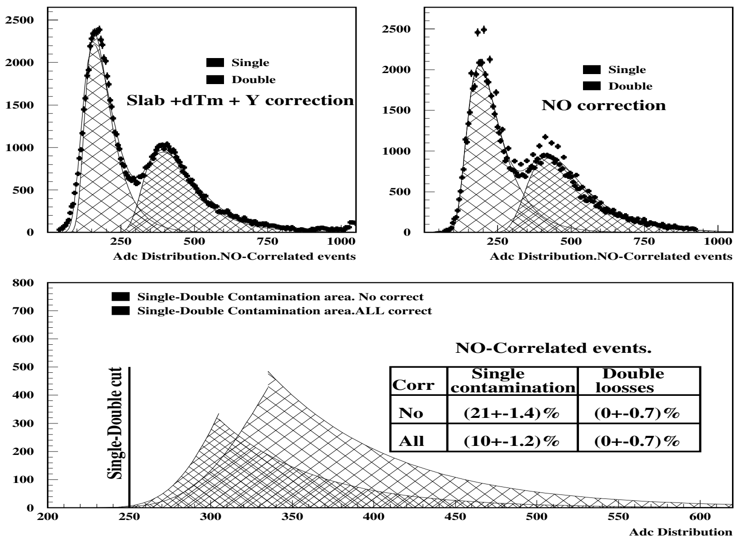

Fig. 35. *The common area between single and double ionization signal are shown before and after corrections.*

8.3 Global effect

Just for completion, a scatter plot shows in another way the effect of the corrections on single-double separation (see figure 36). The increase of the clean area between single and double ionisation reflex the goodness of the correction method.

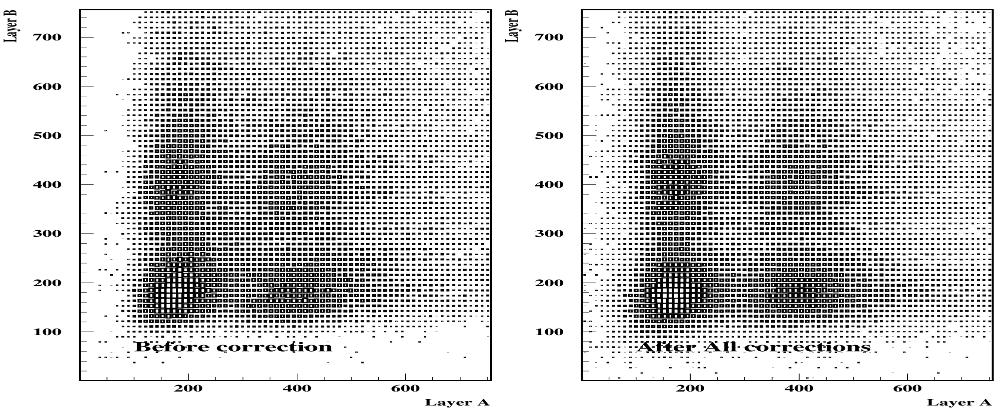

Fig. 36. *Layer A vs Layer B ADC distribution before and after correction.*

9 Some consideration about the relative momentum Q

In this section we want to check how the single ionisation contamination affect the relative momentum distribution. For this purpose the samples following are selected:

. **Single-Single sample** The amplitude associated to a particle is compatible with single ionisation signal in both A and B layers. The cut applied is 200 in each of them.
. **Single-Mixed sample** The amplitude associated is compatible with single in one of the detector layers and compatible with double in the other.
. **Double-Double sample** The amplitude is compatible with double ionisation in both layers. The cut is defined in 400 count in each of them.
. **Overflow sample** The amplitude is in overflow in at least one of the layers.

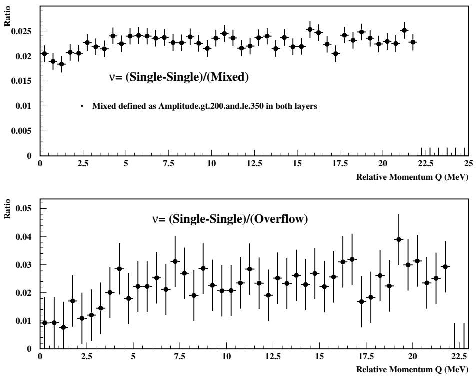

Fig. 37. *On the top, Q distribution versus the ratio between Single-Single and Single-mixed sample. The same on the bottom for single-single-Overflow sample.*

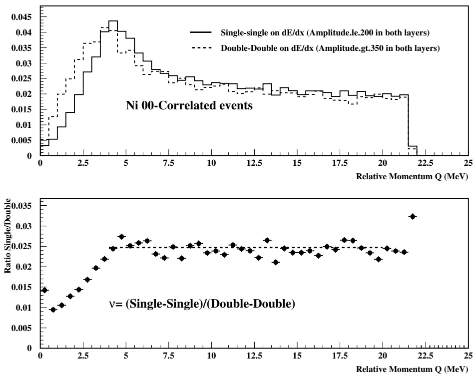

Fig. 38. *On the top, Q distribution for single-single and double-double sample. The area is normalised to unity. On the bottom the ratio between both samples.*

Figure 37 shows the ratio between the number of single-single ionisation events and the number of mixed events on the top. The same figure shows on the bottom the ratio between single-single and overflow events. The main remarks are :

a.- The ratio is constant for Q greater than 4 MeV which correspond to accidental sample.
b.- The relative momentum distribution for single-single events sample is shifted to high values.

Also, in figure 38, the ratio between single-single and double-double ionisation for different momentum distribution ranges is shown. The obtained results are similar to the disccused above.The behaviour was expected. Concluding, the contamination of single events modify the relative momentum distribution, mainly in the low Q region. For this reason, the single contamination must be as smaller as permited.

10 Results comparison with Platinum target 1999 data

The data obtained during 1999 with Platinum target are the better understood.For this reason, we can use its to check if:

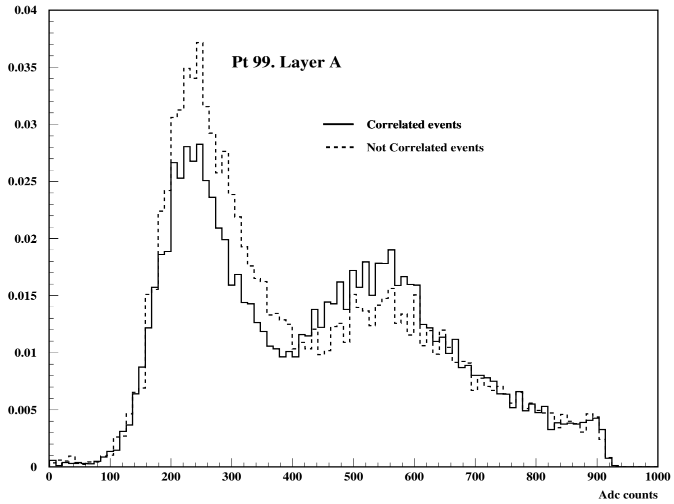

Fig. 39. *ADC distribution for correlated and not-correlated events. Pt target.*

a.- The ADC dependence with dTm appears. (Remember that in 99 the gate 70 ns instead of 56 ns in 2000).In other words, if the explanation above is rigth.

b.- The ADC dependence with the impact position of the particle along the element can be corrected using the proposed method (the dependence is due to the attenuation ligth and then related to the detector construction).

Figure 39 shows the ADC distribution for correlated and not correlated on time events. No differences are observed.The total charge detected is higher than the observed during the 2000 data taking for both samples. The signal lost due to the reduction applied during the 2000 to the readout gate seems to be responsible for the time dependence observed.

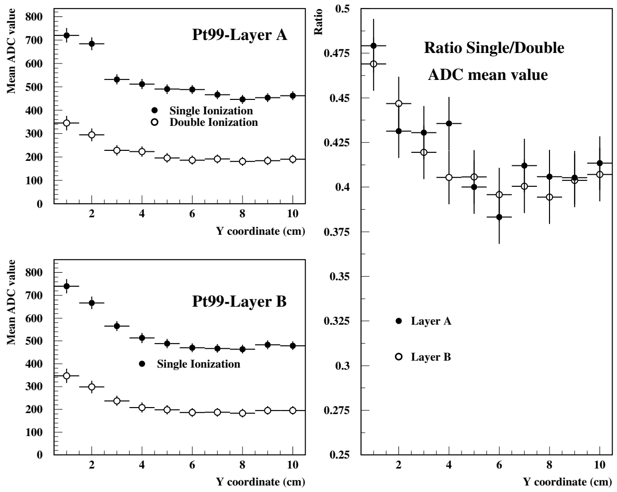

Fig. 40. *ADC distribution for correlated and not-correlated events. Pt target.*

Finally figure 40 shows the dependence of the signal collected with the impact position of the particle along the Y co-ordinate. The method proposed above to correct 2000 data is applied. The obtained fit parameters are in good agree whitin the experimental errors as expected (see figure 41).

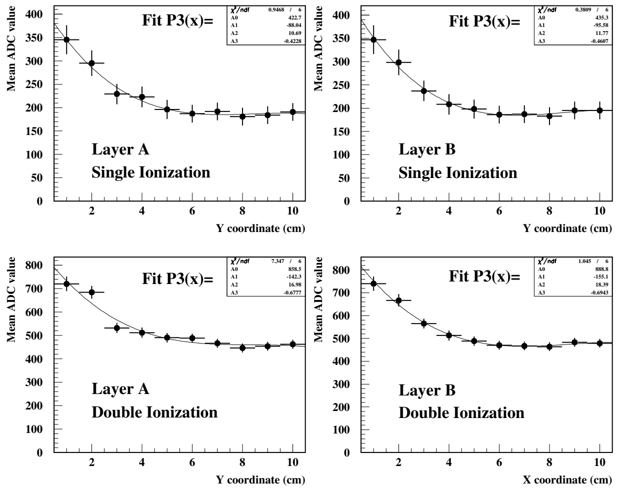

Fig. 41. *ADC distribution for correlated and not-correlated events. Pt target.*

11 Conclusions

A sample of good pair events corresponding to 240 millions triggers has been analysed in order to align the dE/dx detector signals. The main results are:

1.- Detector inhomogeneities can be corrected element per element. The correction is applied as a simple translation. The maximum correction is 10 ADC counts.

2.- Detector response dependence with the impact position of the particle along each element can be corrected using a polynomial function ($P^3(Y)$) fit. The ADC distribution width improves by $6 \pm 2\%$ independently of the treated sample.

3.- The observed asymmetry between correlated and not correlated events the ADC distributions is studied. A plausible explanation can be a not optimised ADC time delay with respect to the readout gate. The effect can be corrected using a polynomial function $P^1(dTm)$ fit, where dTm is the time difference between the 2 particles from the pair. The width improvement is evaluated to be $15 \pm 3\%$ for the not correlated events sample. No effect is observed for the correlated on time pairs.

4.- The detector response looks independent from either the momentum or the charge of the particle hitting the sensitive area.

5.- The full correction global effect induces a 50% reduction of the single contamination in the double ionisation sample.

6.- The predictions of both A and B layers are compared for a single and double ionisation event sample.

    $23 \pm 2\%$ of single ionisation candidates are shown as double ionisation signal in one of the layers. A pileup effect can be the main cause.

    $34 \pm 4\%$ of double ionisation candidates are corrected as single ionisation signal in one of the layers. In 20% of cases the second signal is found in an adjacent element. $14 \pm 4\%$ are compatible with the detector gaps.

7.- A not negligible difference between the relative momentum distribution Q for single and double ionisation is seen. The observed effect is localised in the very low Q region, where our sensitivity is must be better. This fact suggests **a cut criteria hard enough to avoid as much as possible the single contamination** .

i

12 Acknowledgements

I wish to acknowledge Daniel Drijard for a lot of useful discussions and support.

13 References

1.- C. Detraz, M. Ferro-Luzzi and J.-M. Perreau, *Tests of ionisation hodoscope elements* Dirac internal note 96-05.

2.- C. Detraz, M. Ferro-Luzzi and J.-M. Perreau, *Tests of ionisation hodoscope elements (part 2)* Dirac internal note 96-06.

3.- D. Drijard and M. Ferro-Luzzi, *Tests of ionisation hodoscope elements (part 3)* Dirac internal note 96-13.

4.- C. Detraz, D. Drijard, M. Ferro-Luzzi (CERN) and V. Komarov (JINR), *The ionisation hodoscope: performance and characteristics of the first module*, Dirac internal Note 97-09.

5.- Daniel Drijard. Internal communication.

6.- Anatoly Koulikov. Internal communication.

14 Appendix A:Practical details

1.- **How compute the number of photoelectrons:** The ADC distribution is fitted with a gaussian(Internal PAW fit). 20 bins are fitted (only 6 after the peak). One bin correspond to 10 ADC counts.

2.- **How compute the contamination area:** The total ADC distribution is fitted using a double Landau distribution (see look *.../alopeza/production/FUNC.f*).The common area in calculated using the SIGMA package (see PAW).

3.- **How apply the corrections for the standard analysis:**

3.a.- The element by element alignment is included into the prepfn as 2 vectors (dedxA(16) and dedxB(16), look on *.../alopeza/production/prepfnw.kumac*).

3.b.- Both time and Y co-ordinate dependence are included in fillhfnXX (look on *.../alopeza/production/fillhfn50.f*).

Finally, the information to be contain into the DATABASE: